Journal of Directed Energy, **3**, Fall 2008, 15–24

Large-Spot Material Interactions with a High-Power Solid-State Laser Beam

C. D. Boley,* S. N. Fochs,† and A. M. Rubenchik‡

Lawrence Livermore National Laboratory, Livermore, California 94551

We study the material interactions produced by the beam of a 25-kW solid-state laser in experiments characterized by relatively large spot sizes (~3 cm) and the presence of airflow. The targets are iron or aluminum slabs of thickness 1 cm. In the experiments with iron, we show that combustion plays an important role in heating the material. In the experiments with aluminum, we observe a sharp transition from no melting to complete melt-through as the irradiance on target increases. A layer of paint greatly reduces the requirements for melt-through. We explain these effects and incorporate them into an overall computational model.

KEYWORDS: Airflow, Combustion, High average power, Large spot size, Solid-state laser

Nomenclature

C	specific heat
I	laser irradiance
T	temperature
T_c	combustion initiation temperature
U_0	wind speed
x_o	thickness of oxide layer
α	optical absorptivity
η	shear viscosity
κ	thermal conductivity
ρ	density
σ	shear stress

1. Introduction

Solid-state lasers with high average power are of great current interest. Our laboratory at Lawrence Livermore National Laboratory has been developing such lasers for defense applications during the past decade. Here we are concerned with a device[9,10] containing four diode-pumped ceramic Nd:YAG slabs, which produces approximately 25 kW of time-average power at a wavelength of 1.064 μm. Routine operation for 10 s has been

Received October 8, 2007; revision received August 21, 2008.

*Corresponding author; e-mail: boley1@llnl.gov.

†Current address: Metal Improvement Company, Livermore, CA 94551; e-mail: Scott_Fochs@metalimprovement.com.

‡E-mail: rubenchik1@llnl.gov.

demonstrated. The laser operates at a pulse repetition rate of 200 Hz, producing pulses of energy about 125 J and length about 0.5 ms, for a duty factor of about 10%. With the addition of another slab and an increased diode duty factor, the laser has also achieved 67 kW for 0.25 s (as limited by diode capabilities). During lasing operations, the laser stores waste heat in the solid-state slabs. In field applications, the hot slabs would be interchanged with cool slabs and rapidly cooled.

Our laser power corresponds to the power on target for a tactical defense system having approximately twice that power (50 kW) because projected losses due to the beam director and propagation are typically of order 50%. The spot size ($\sim$3 cm) is representative of that expected for many field targets. To simulate field conditions, airflow of about 100 m/s was used in most of the experiments. Hence our results are applicable for the description of laser–matter interaction of more practical and powerful systems.

We have explored the material interactions of our lasers, including high-explosive initiation, at some length.[2–5] Because the thermal conduction length between pulses is small compared to typical target dimensions, the macroscopic heat distribution is readily seen to be governed by the time-average power, as opposed to the peak power[5] (the latter is, of course, about 10 times the former). Our predictive capability is embodied in a computational model. With this model, devices operating near 100 kW have been projected to be effective in defense against tactical projectiles.[2,4,5]

The goal of the present paper is twofold: to study laser–matter interactions under conditions approximating those in the field (large spot size, irradiance below vaporization threshold, airflow), and to use the experiments to benchmark and calibrate our code and to include the new physics effects in modeling.

Laser–matter interactions for defense applications have been studied since at least the 1970s, and a great deal of data has been collected (see, e.g., an extensive review[7] and also the lectures[1]). The data are sensitive to the laser wavelength, pulse duration, laser irradiance, materials, and so forth. Because of the impetus for a 100-kW solid-state laser, studies such as ours of large-spot, multikilowatt interactions at 1 μm are particularly timely.

Our experiments employed thick (1 cm) iron and aluminum coupons. For iron, this approximates the shell thickness of some mortars. For Al, this is related to the wall thickness of wing fuel tanks. The beam footprint was square, with nearly uniform irradiance over the spot. Examination of the laser imprint after several pulses showed no visible patterns. According to calorimetry, the pulse-to-pulse energy varied by less than 5%. In all experiments, the time-average power was 25 kW and the irradiation time was 5 s. The experimental setup near the target is shown in Fig. 1.

In the case of iron, we demonstrate that, under these conditions, combustion plays an important role in facilitating material heating. This was also suggested by earlier experiments at lower power.[3] For aluminum, we find that target damage sharply changes with increased irradiance. At about 3 kW/cm^2, no cratering or melting is observed. At twice this irradiance, however, the coupon rapidly melts through. This effect is explained by the large thermal conductivity of Al. The behavior is altered by a paint layer, which serves to increase the absorption. As a result, Al targets differ from iron in sensitivity to paint. We show that our simulations are consistent with these observations.

2. Interactions with Iron Coupons

We begin by describing the irradiation of iron coupons. These were made from mild steel 1020. The coupon size (5 $\times$ 7.5 cm^2) was sufficiently large to eliminate boundary effects.

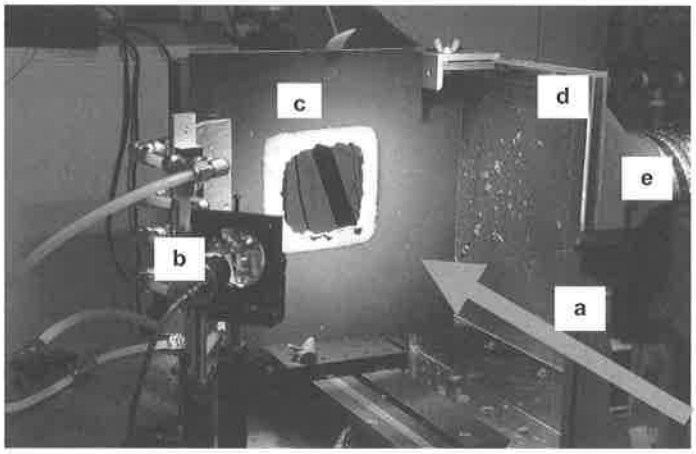

Fig. 1. Experimental setup, immediately after irradiation of a target. The laser is out of view, to the lower right. The designated elements are (a) beam path, (b) blower assembly, (c) target (in this case, a metal sheet with a 13 × 13 cm^2 spot size), (d) coupon pieces on a screen, and (e) suction assembly.

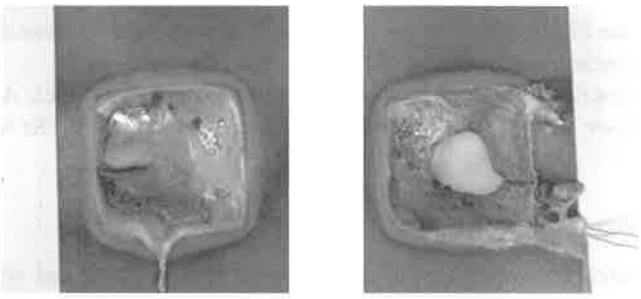

Fig. 2. Iron coupons after irradiation experiments. Left, no flow; right, airflow. The beam spot size is 3 × 3 cm^2.

The spot size was 3 × 3 cm^2, corresponding to an average irradiance of about 2.8 kW/cm^2. At this irradiance, the energy losses to vaporization are insignificant. The temperature history at the rear center of a coupon was recorded with a thermocouple. Experiments were conducted for three cases: (1) no flow past the surface, (2) airflow at about 100 m/s, and (3) nitrogen flow at this speed. Melt-through was observed with airflow but not with nitrogen flow or in the absence of flow. The difference between no flow and airflow is evident in the coupon photographs of Fig. 2. Note the viscous dripping under gravity in the former case.

More detailed information is revealed in the thermocouple readings shown in Fig. 3. This shows that there is a striking difference between airflow and nitrogen flow. Whereas each involves melt removal by the wind, the temperature is visibly enhanced by airflow. From measurements of the removed material, we estimated Q^*, the amount of laser energy to remove unit mass of material. We obtain $Q^* = 5.7$ kJ/g without flow. With nitrogen flow, we have $Q^* = 4.7$ kJ/g, whereas with airflow we have $Q^* < 3.2$ kJ/g (an upper bound, because melt-through was achieved). The decrease from no flow to nitrogen flow is explained by

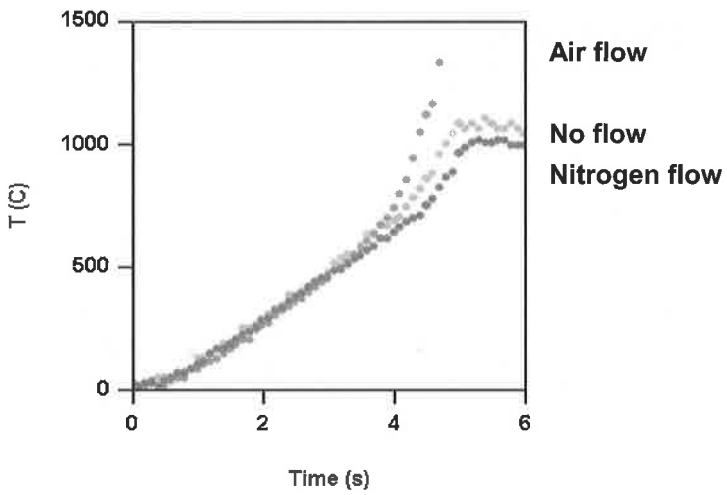

Fig. 3. Thermocouple readings for the iron coupons. The beam was turned off at 5 s. The data have a maximum jitter about the mean of about 10 deg.

melt removal. The decrease from nitrogen to airflow is attributed to combustion. Here we wish to explain the difference between airflow and nitrogen flow in more detail. To do so, we turn to our interaction model and add combustion effects.

Our model[5] describes physical processes within an irradiated target. After absorption of the incident laser energy, heat is conducted through the target via the heat conduction equation,

$$\rho C \frac{\partial T}{\partial t} = \nabla \cdot \kappa \nabla T + S, \tag{1}$$

where S is a source term particular to the problem. Melt removal and wind cooling are included in the model. Calculations are performed in two-dimensional (r, z) symmetry, relative to the beam centerline. The model accesses a database of temperature-dependent material properties, including the heat capacity C, the thermal conductivity κ, and the absorptivity at the laser wavelength.

We have added combustion effects to this model by considering a thin oxide layer of thickness x_o, situated on a melt layer. This enters into the boundary condition for the heat conduction equation via

$$\kappa \frac{\partial T}{\partial z} = \alpha I + W_c \dot{x}_o, \tag{2}$$

where α is the temperature-dependent surface absorptivity and W_c is the latent heat of the combustion reaction, per volume. The z axis is oriented such that the temperature gradient is ordinarily positive. The growth of the oxide layer is governed by the equation[8]

$$\dot{x}_o = (D/x_o) \exp(-T_c/T), \tag{3}$$

where T_c is the initiation temperature and D is an empirical parameter. This equation describes the oxygen diffusion through the oxide layer. The self-consistent description of laser-induced combustion has been the subject of many studies.[8] In our case, the situation is greatly simplified by the fact that the wind removes the melt layer along with the oxide

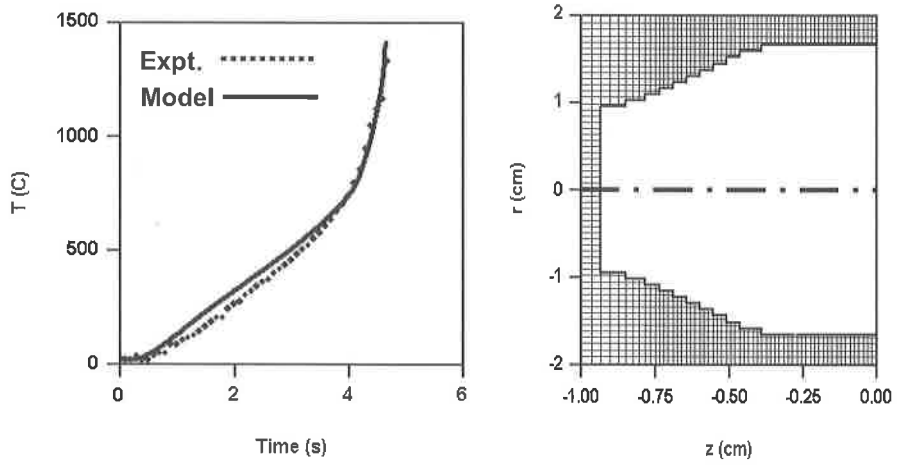

Fig. 4. Left: Comparison of experimental and calculated temperatures on the rear center of an iron coupon, with airflow. Right: Calculated hole profile immediately before breakthrough. A circularly symmetric geometry is used.

layer. Thus the oxide thickness and the rate of oxidation are determined primarily by wind effects rather than by complex thermochemical reactions. Equation (3) is to be evaluated at the time required for melt removal, which is of order a/u, where a is the spot size and u is the melt speed at the melt surface. The latter, in turn, is of order $\sigma h/\eta$, where h is the melt depth, η is the shear viscosity of the melt, and σ is the shear stress at the surface. We assume a turbulent boundary layer in which the shear stress is given by the von Kármán expression[6] $\sigma = c\rho_0 U_0^2$, where ρ_0 and U_0 are the density and speed, respectively, of the wind. The overall factor c is insensitive to details of the flow and depends logarithmically on the flow velocity. Finally, then, the boundary condition (2) takes the form

$$\kappa \frac{\partial T}{\partial z} = \alpha I + Q_c U_0 \exp(-T_c/2T). \tag{4}$$

Thus the heating flux due to combustion, as summarized in the last term, is proportional to the wind speed and increases exponentially with the surface temperature. The parameter Q_c comprises both material and flow parameters. Unfortunately, the parameters Q_c and T_c are not available in the literature. Therefore we resorted to fitting them from our data. The model neglects the change of oxide reflectivity and also the effect of flow structure on melt removal. We hope that the limits of applicability can be ascertained by more detailed experiments.

Figure 4 shows the thermocouple temperature as calculated by this model, with $Q_c = (0.8\ \text{kW/cm}^2)/(10^4\ \text{cm/s})$ and $T_c = 4{,}000$ K. It agrees well with experiment. (In such runs, we used a fixed T_c, as estimated from energetics, and varied Q_c for the best visual fit. On this basis, the quoted Q_c is estimated to be accurate within about 20%.) Overall, combustion adds approximately 35% to the deposited energy for our experiment. The code cannot reliably predict the final shape of the cavity, because this is determined in part by gravity effects and lip motion.

In Fig. 5 we show the result of a calculation with wind but without combustion. As expected from our picture, this agrees with the laboratory result for nitrogen flow.

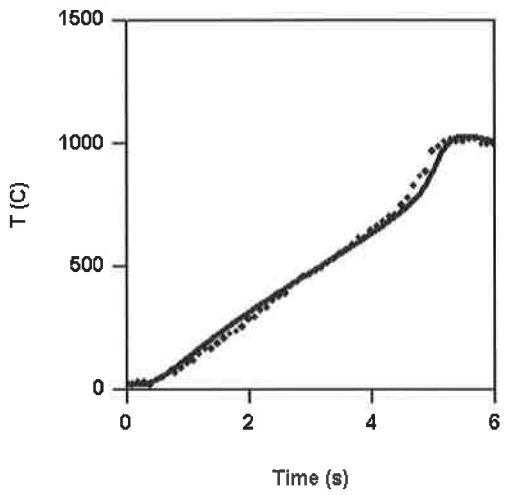

Fig. 5. Comparison of experimental and calculated temperatures on the rear center of an iron coupon, with nitrogen flow.

The modified boundary condition (4) makes it possible to estimate the effect of combustion on lethality involving rapid cook off. Of course this typically occurs before the material is melted through. The results will be published separately.

Our experiments were performed with a wind speed of about 100 m/s. Unfortunately, the speed could not be increased. From Eq. (4), we predict that the role of combustion should increase with projectile speed. Thus it would be very interesting to do experiments with a higher wind speed, as would be pertinent, say, for some rockets.

3. Interactions with Aluminum Coupons

Next we turn to the irradiation of aluminum coupons. These were made from the alloy Al 6061. Again the coupon size (12.5×12.5 cm^2) was sufficient to eliminate boundary effects. As in the preceding section, the coupon thickness was 1 cm. The temperature history at the rear center of a coupon was recorded with a thermocouple. Combustion is not important for aluminum because the oxide layer is sufficiently dense to suppress combustion.

Before we present the results, let us discuss what we expect to observe. For iron coupons, the temperature typically has a strong gradient near the edge, owing to the relatively low thermal conductivity. Consequently, a thin melted layer is continuously removed by the wind. A painted layer will be removed in the very beginning of the laser target interaction. As a result, paint would not be expected to have a significant effect on laser penetration.[8]

The situation with Al is different. The thermal conduction time through the coupon is about 0.25 s, so the temperature profile will be practically uniform across the coupon. When the front surface starts to melt, the rear surface is also close to the melting point. As a result, one can expect a sharp change in the behavior with increase in irradiance, for a given irradiation time. When the irradiance is insufficient to melt the surface, the laser pulse causes essentially no surface modification. Once the power is high enough to start melting, though, practically the entire irradiated slab is melted and removed by the wind. Thus we expect a sharp transition from no effect to melt-through as the laser irradiance increases. The experiments are consistent with this description.

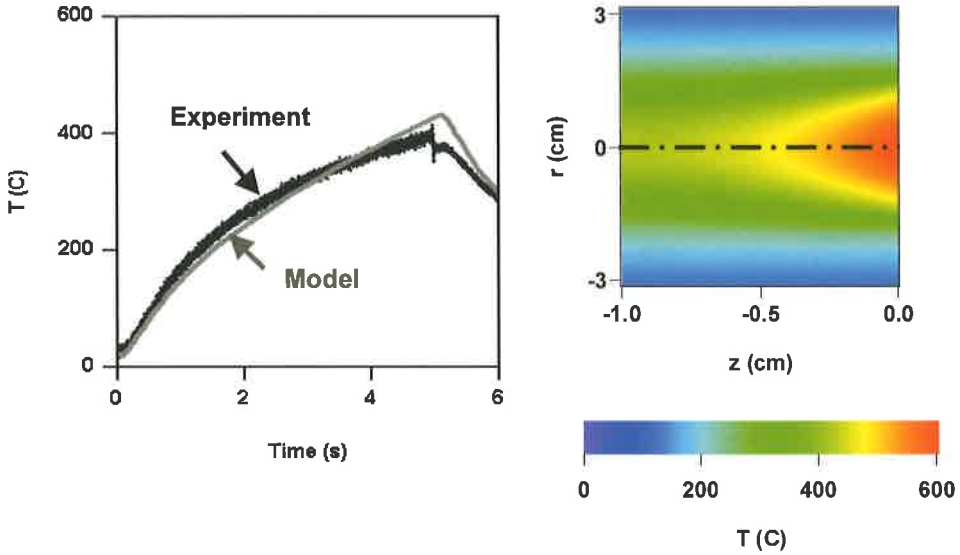

Fig. 6. Irradiation of a 1-cm aluminum coupon by 25 kW for 5 s, with a spot size of 2.8×2.8 cm^2. Left: Temperature trace of a thermocouple on the rear center, along with the model calculation. Right: Calculated temperature distribution immediately before the beam is turned off. The beam enters from the right.

Figure 6 shows the experimental temperature trace for a spot size of 2.8×2.8 cm^2, corresponding to an irradiance of about 3.2 kW/cm^2. During the irradiation time, the temperature grows to a maximum of about 400°C, with no melting. Also shown is the model calculation, which agrees well with the data throughout the experiment. The right-hand plot shows the temperature distribution at maximum. This clearly exhibits two-dimensional effects, owing to the large thermal conductivity. To fit the data we used a mildly temperature-dependent absorptivity, which increased from 0.13 at room temperature to 0.24 at the melting point. The linear growth with temperature is consistent with the Drude model.[8] The room-temperature value exceeds the normally quoted value of a few percent for pure aluminum, because of surface roughness, but is less than the cited value of 0.2 for Al 2024 alloys.[1]

In the next experiment, the spot size on the coupon was decreased to 2×2 cm^2. As shown in Fig. 7, both experiment and model now give material melt-through at about 3 s. This suggests that our code description of melt removal provides a reasonable description of the experiments.

The presence of paint greatly changes the interaction with an aluminum target. Paints have a complicated composition and are available in many varieties, but in most cases the absorptivity of the painted surface is much higher than that of bare aluminum. In an elementary model, paint acts as a thin layer with a high absorptivity and a low thermal conductivity. To see its effect on aluminum, we irradiated a painted coupon, with a spot size of 3×3 cm^2, for 5 s. The paint was a dull gray. It was a commercial aerosol spray, without primer. As we noted earlier, a slightly smaller spot size, 2.8×2.8 cm^2, failed to produce melting. The painted coupon, however, absorbed appreciably more energy and melted through somewhat after 2 s, as shown in Fig. 8. (The thermocouple failed at 2 s because of the loss of material strength below the melting temperature.) This experiment suggests

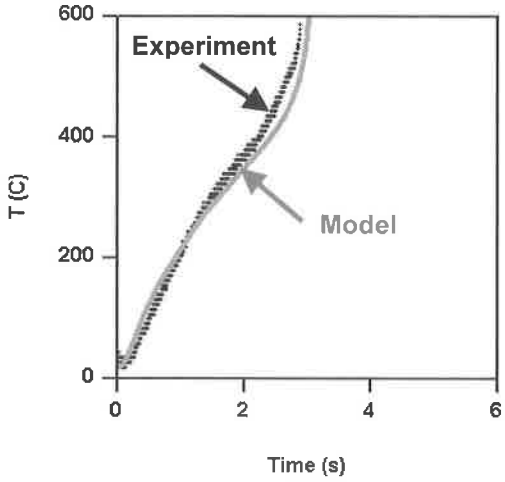

Fig. 7. Temperature trace at the rear center of an aluminum coupon, during irradiation with a spot size of 2×2 cm^2.

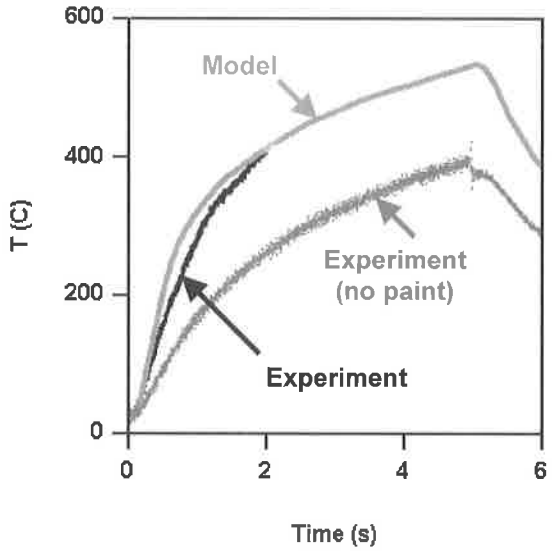

Fig. 8. Top two lines: Temperature traces (model and experiment) for the irradiation of a 1-cm painted aluminum coupon by 25 kW for 5 s, with a spot size of 3×3 cm^2. The thermocouple failed at 2 s. The bottom line gives the temperature trace for a 2.8×2.8 cm^2 spot with no paint, from Fig. 6.

that the paint survived approximately to the point at which the aluminum began to melt. Because at this moment the temperature profile across the target is close to the melting point, a painted layer should greatly decrease the power required to penetrate an aluminum target.

Also shown in Fig. 8 is the result of a two-dimensional model calculation, in which the paint was treated as a 200-μm layer with an absorptivity of 0.5, a thermal conductivity of

0.08 W/(cm K), and a volume specific heat of 1 J/(cm^3 K). The thermal conduction time across the paint layer, about 1 ms, is short compared to the time scale of the experiment. The paint was assumed to decompose at 500°C. Numerically, a paint cell was removed when it reached this temperature. The temperature trace is reasonably close to experiment, as shown in Fig. 8. This result confirms that our simple model of this paint may be adequate. The paint model is admittedly idealized because, for example, carbonization typically increases the absorptivity. However, we would not expect the results to be very sensitive to such refinements.

4. Conclusions

We have described experiments and modeling concerning the interactions of a high-power solid-state laser with target materials. The laser delivered 25 kW for 5 s, on coupons of iron and aluminum having a thickness of 1 cm. The spot sizes were relatively large, about 3 × 3 cm^2. Airflow at about 100 m/s was present.

For an iron coupon, we showed that combustion plays an important role in adding to the material heating. This effect was absent in nitrogen flow. For aluminum, we found a strong dependence on the incident laser irradiance. At approximately 3.2 kW/cm^2, no melting was observed, because of efficient lateral heat conduction. At about 6.2 kW/cm^2, however, the coupon rapidly melted through. This behavior was explained in terms of rapid heat conduction along the axial direction. Paint was observed to increase appreciably the absorption. Thus it should decrease the power needed for melt-through.

Finally, we showed that these results are reproduced by a comprehensive computational model, which includes the temperature-dependent thermal conduction, melting and melt removal by the wind, wind cooling, and iron combustion. With the modifications calibrated by these experiments, the model can be used for further applications.

5. Acknowledgment

We are pleased to acknowledge our debt to R. M. Yamamoto, the chief engineer for the laser project.

References

[1]Beraun, J. E., "Laser Materials Effects," Short Course, Directed Energy Professional Society, Fifth Annual Directed Energy Symposium, Monterey, CA, November 12, 2002; Beraun, J. E., and J. Evanoff, "Laser Effects and Vulnerability Assessment Process," Short Course, Directed Energy Professional Society, Sixth Annual Directed Energy Symposium, Albuquerque, NM, October 20, 2003.

[2]Boley, C. D., S. N. Fochs, and A. M. Rubenchik, "Lethality of a High-Power Solid-State Laser," Directed Energy Professional Society, Ninth Annual Directed Energy Symposium, Albuquerque, NM, October 30–November 3, 2006.

[3]Boley, C. D., and A. M. Rubenchik, "Modeling of High-Energy Pulsed Laser Interactions with Coupons," University of California, UCRL-ID-151857, February 6, 2003.

[4]Boley, C. D., and A. M. Rubenchik, "Lethality of High-Power Solid-State Lasers on High-Explosive Targets," Directed Energy Professional Society, Eighth Annual Directed Energy Symposium, Lihue, HI, November 14–18, 2005.

[5]Boley, C. D., and A. M. Rubenchik, J. Directed Energy **2**, 97 (2006).

[6]Landau, L. D., and E. M. Lifshitz, *Fluid Mechanics*, Pergamon Press, Oxford, UK (1978).

[7]Physical Sciences, Inc. (W. T. Laughlin, H. H. Legner, M. G. Miller, E. R. Pugh, and G. A. Simons), "Laser Materials Effects and Lethality Handbook," PSI-1302/TR-1615 (1999).

[8]Prokhorov, A. M., V. I. Konov, I. Ursu, and I. N. Mihailescu, *Laser Heating of Metals*, Adam Hilger, New York (1990).

[9]Soules, T. F., M. D. Rotter, S. N. Fochs, R. M. Yamamoto, C. Parks, and B. Bhachu, "Ceramic Nd:YAG—Current Material of Choice for SSHCL," Directed Energy Professional Society, Eighth Annual Directed Energy Symposium, Lihue, HI, November 14–18, 2005.

[10]Yamamoto, R., B. K. Allen, R. Allmon, K. Alviso, B. Bhachu, C. Boley, R. Combs, K. Cutter, S. Fochs, S. Gonzales, R. Hurd, K. LaFortune, W. Manning, R. Merrill, L. Molina, J. Parker, C. Parks, P. Pax, A. Posey, M. Rotter, B. Roy, A. Rubenchik, and T. Soules, "A Solid State Laser for the Battlefield," 25th Army Science Conference, Orlando, FL, November 27–30, 2006 (UCRL-CONF-225230).

The Authors

Dr. Charles D. Boley received his S.B. and Ph.D. in physics from the Massachusetts Institute of Technology, in 1966 and 1971, respectively. Since 1986, he has been a physicist at Lawrence Livermore National Laboratory. There he has modeled phenomena in laser isotope separation, laser–materials processing, lasers for inertial fusion (including the plasma-electrode Pockels cell and spatial filter pinholes, in the National Ignition Facility), short-pulse lasers, and high-average-power, solid-state lasers.

S. N. Fochs. Biography not available at press time.

Dr. Alexander M. Rubenchik received his Ph.D. in theoretical physics from the Institute of Nuclear Physics, Novosibirsk, in 1974. He received the Dr.Sci. degree from the Space Research Institute, Moscow, in 1983. Currently, he is a physicist at Lawrence Livermore National Laboratory. His main scientific interests are in the physics of laser–matter interactions, nonlinear optics including studies of optical damage, and plasma physics. He is a member of the DEPS.

Journal of Directed Energy, **3**, Fall 2008, 25–37

Resistive Sensor for High-Power Microwave Pulse Measurement

Mindaugas Dagys,* Žilvinas Kancleris,† and Rimantas Simniškis‡

Microwave Laboratory, Semiconductor Physics Institute, A. Goštauto 11, Vilnius LT-01108, Lithuania

A resistive sensor (RS) devoted to the measurement of a high-power microwave (HPM) pulse is presented. The performance of the RS is based on the electron-heating effect in semiconductors. It can measure HPM pulses directly; it is resistant to large power overloads and demonstrates very good long-term stability. The RS can produce an output signal of the order of a few tens of volts without any amplification circuit, and it can measure nanosecond-duration HPM pulses. Different types of the RS developed, manufactured, and tested in our laboratory are presented. They are the cross-waveguide RS for an intermediate pulse power level, the waveguide-type RS with diaphragm for HPM pulse measurements, the coaxial-type RS for the measurement of microwave pulses in a wide frequency range, and the RS for a millimeter-wave region.

KEYWORDS: Electron heating, High-power microwave pulse measurement, n-Si, Sensors

1. Introduction

High-power microwave (HPM) pulse generators are being intensively studied in laboratories as well as being manufactured by industry. Owing to the increasing growth in the use of HPM sources, their potential threat to electronic equipment should be taken into account. On the other hand, intentional attacks on the electronic infrastructure using an HPM source as a directed energy weapon might be expected, and possible disturbances with fatal consequences for civil and military systems should be considered. Both these trends demand that tests of electronic equipment be performed at higher pulse power levels. This in turn brings forward new requirements for sources and sensors that are used in tests.

Traditionally, calibrated diodes are employed to measure the power of microwave pulses, but they can handle only a very low power level. Therefore, before being measured with the diode the HPM pulse has to be strongly attenuated. An additional attenuation results in a decrease in measurement accuracy. Moreover, problems may arise when measuring a small dc signal from the diode due to the presence of stray pickup and electromagnetic interference, which are typical of the environment of HPM sources. Novel electro-optic measurement techniques[10] can be applied efficiently in the HPM environment, but the external sensitive equipment (such as lasers, polarizers, and other optics) restricts application areas.

Received January 17, 2008; revision received June 9, 2008.

†Corresponding author; e-mail: kancleris@pfi.lt.

*E-mail: dagys@pfi.lt.

‡E-mail: rimsim@pfi.lt.

An alternative HPM pulse measurement device, a resistive sensor (RS),[3] helps to overcome these difficulties. The performance of the RS is based on the electron-heating effect in semiconductors. A sensing element (SE) of the RS is placed in the transmission line. The electric field of the HPM pulse heats electrons in the SE; its resistance increases, and by measuring this resistance change, the HPM pulse power is determined. Such a compact and rigid sensor can measure HPM pulses directly, can produce a high output signal, is overload resistant, and demonstrates very good long-term stability. In this paper, different types of RS are presented. The paper is organized as follows. In the second section the principle of performance of the RS and its sensitivity are described. The actual design of the RS for the rectangular waveguide is presented in the third section. The coaxial RS is described in the fourth section.

2. Resistive Sensor

The investigation of semiconductors subjected to a strong electric field began more that 50 years ago when Ryder and Shockley[7] found that for large electric fields, the current deviates from the dependence predicted by Ohm's law. It was understood that in a strong electric field, electrons gain additional energy from the electric field and a new steady state is established with mean electron energy greater than that of the equilibrium one. As a rule, heated electrons are more frequently scattered by lattice imperfections (phonons), and the resistance of the semiconductor usually increases. It was realized that the resistance change in a strong electric field could be used for pulsed-microwave-signal measurement. By placing a semiconductor sample in the transmission line and measuring the resistance change occurring when the electric field of the microwave pulse heats electrons in the sample, the microwave pulse power in the transmission line can be determined.

2.1. Sensing element and output signal

Because the resistance change of the semiconductor is a basis for a RS's operation, for HPM pulse measurement we actually use a resistor made from n-type Si. The SE is a bar- or plate-shaped piece of Si with ohmic contacts. Impurity diffusion followed by metal evaporation is used to form contacts. A typical sample length is 0.1–10 mm. Depending on the particular application, various ingots of silicon with different specific resistances are used.

To measure the resistance change in the microwave electric field, the SE should be connected to a dc circuit. Therefore, the output signal from the RS being measured using a high-input resistance-measuring unit can be expressed in the following way:

$$U_S = U_0 \frac{\Delta R}{R}, \tag{1}$$

where U_0 is a dc voltage drop on the SE and $\Delta R/R$ is a relative resistance change in the SE, obtained by averaging the instantaneous current over the period of the microwave electric field. In a low power limit, the strength of an average microwave electric field in the SE is sufficiently small. Therefore, its resistance change can be expanded in a power series of the electric field and only the first nonvanishing term can be taken into account,[3] thus yielding

$$\frac{\Delta R}{R} = \beta^*(f)\langle E\rangle^2, \tag{2}$$

Table 1. Typical values of phenomenological parameters characterizing current voltage characteristics of n-Si at room temperature for different specific resistance ρ materials

ρ, Ω·cm	β_0^*, cm^2/V^2	k_n^*	τ_ε, s
5	9.0×10^{-8}	3.0	2.9×10^{-12}
20	9.3×10^{-8}	3.4	
200	10.1×10^{-8}	4.3	

where $\beta^*(f)$ is frequency dependent, so-called, an effective warm-electron coefficient defining a deviation of the current-voltage characteristic from Ohm's law, and $\langle E \rangle$ is an average amplitude of the electric field in the SE. The region where equation (2) expression is valid is called a warm-electron region. In general, the effective warm-electron coefficient is frequency dependent and this dependence accounts for the influence of electron-heating inertia on the resistance change in the microwave electric field:

$$\frac{\beta^*(f)}{\beta_0^*} = \frac{1}{3}\left[1 + \frac{2}{1 + (2\pi f \tau_\varepsilon)^2}\right], \tag{3}$$

where β_0^* is a value of the effective warm-electron coefficient in a low-frequency region and τ_ε is a phenomenological energy relaxation time. Typical values of β_0^* and τ_ε for n-Si at room temperature are collected in Table 1. From Eq. (3) one can find that at 12 GHz the decrease of β^* due to heating inertia is roughly 3%. Therefore, the influence of heating inertia on β^*can be neglected up to and including X band.

Experimental investigations have revealed that the warm-electron approximation holds well up to the electric field strength around 1 kV/cm, at which $\Delta R/R$ is of the order of 10%. At a higher electric field, there is a considerable deviation of the relative resistance change from the dependence predicted by expression (2). It was found that over a wider range of the electric field strength, the resistance change is described by the following empirical relation, with two adjustable parameters:

$$\frac{\Delta R}{R} = \frac{\sqrt{1 + 4k_n^* \beta^* \langle E \rangle^2} - 1}{2k_n^*}, \tag{4}$$

where k_n^* describes the deviation of $\Delta R/R$ from quadratic dependence predicted by Eq. (2). Typical values of k_n^* for n-type Si at room temperature are presented in Table 1.

2.2. Sensitivity

Let us consider the sensitivity of the RS in the linear region where the output signal of the RS is proportional to the pulse power P propagating in the transmission line. Because the resistance change of the SE is the quantity indicating pulse power level, it is convenient to define the sensitivity ζ of the RS as

$$\zeta = \frac{\Delta R/R}{P}. \tag{5}$$

Definition (5) is not unique. Often sensitivity is defined as a signal-to-power ratio. Taking into account that the signal amplitude depends not only on the dc voltage drop on the SE but on the input resistance of the measurement unit used for the output signal measurement, the proposed definition of the sensitivity is likely more acceptable. Inserting Eqs. (2) and (3) into Eq. (5), one can get the following expression:

$$\zeta = \frac{\beta_0^*}{3}\left[1 + \frac{2}{1 + (2\pi f \tau_\varepsilon)^2}\right]\frac{\langle E\rangle^2}{P}, \tag{6}$$

describing the sensitivity of the RS in the linear region. The average electric field is the only unknown quantity in Eq. (6). Thus determining it, the sensitivity of the RS in the linear region can be calculated. For the calculation of the average electric field in the SE and optimization of the frequency response of the RS, we used the finite different time domain (FDTD) method.[8]

As already mentioned, when measuring power increases, the relative resistance change deviates from the linear dependence [Eq. (5)]. It was well established that $\Delta R/R$ dependence on the pulse power in a wide range of P can be approximated as the second-order polynomial in the following way[3]:

$$P = A\frac{\Delta R}{R} + B\left(\frac{\Delta R}{R}\right)^2, \tag{7}$$

where coefficients A and B are determined by fitting the experimentally measured dependence of $\Delta R/R$ on P with Eq. (7). Comparing Eq. (7) with Eq. (5), one can see that $\zeta = A^{-1}$. Expression (7) can be used as an analytical description of the calibration curve of the RS. When the coefficients A and B for the particular RS are determined, inserting Eq. (1) into Eq. (7), one obtains an expression binding the pulse power P with the measured signal U_s. Making use of such an analytical expression allows us to improve the measurement accuracy when the amplitude of the measured signal falls outside the linear region of the RS.

2.3. DC pulse supply

Considering expression (1), one can see that the output signal linearly grows with the dc voltage drop on the SE. The increase in the dc voltage applied to the SE is limited by sensor heating that worsens the sensor's characteristics. Instead, a pulsed-current source is used. It produces a roughly 120-μs dc pulse. The amplitude of the current is adjusted to get the desirable voltage drop on the SE. After 100 μs when the current pulse starts, the HPM pulse source is triggered. Therefore, the output signal appears as a short video pulse on the pad of the feeding pulse. A differencing circuit cuts the pad, and the useful signal is measured by an oscilloscope. The pulsed-current source provides a significant increase in the output signal from the RS without any amplification circuit.

3. RS in Rectangular Waveguide

Rectangular waveguides are widely used as transmission lines for HPM applications. Therefore, we have focused our attention on the measurement of pulsed power in rectangular waveguides.

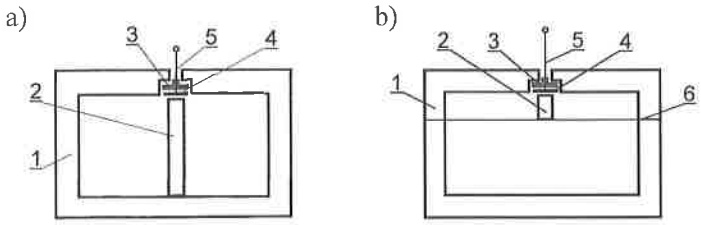

Fig. 1. Schematic views of cross-waveguide-type RS (a) and diaphragm-type RS (b): 1, waveguide; 2, SE; 3 and 4, insulating and metallic washers; 5, output; and 6, diaphragm.

3.1. Cross-waveguide-type RS

A cross-waveguide-type RS is made as a section of a standard waveguide where the SE is mounted. A schematic view of the RS is shown in Fig. 1a. The SE of the RS is placed in the center of the waveguide. It is a bar-shaped piece of semiconductor with ohmic contacts on its ends. The specific resistance of the semiconductor used as the SE is in the range 20–200 Ω·cm. The length of the SE corresponds to the dimension of the narrow wall of the waveguide. The grounded end of the SE is directly connected to the waveguide. The other end of the SE is isolated and connected to the measurement circuit and current source. The RS described above has been mainly used for the measurement of intermediate levels of pulse power (~1 kW) at X band (waveguide size 23×10 mm^2).

Considering the thermal characteristics of the cross-waveguide-type RS, it was shown that some average heating of the SE occurs when it is fed by a sequence of microwave pulses. Electron and lattice heating inertia differ by many orders. Therefore, two kinds of measurements can be performed independently: the measurement of the pulse signal that appears due to electron heating and the measurement of the increase in the average resistance caused by the heating of the SE. The measured pulse signal is proportional to the pulse power, whereas the increase in resistance is proportional to the average power absorbed in the SE. This means that the cross-waveguide sensor can serve as a pulse power meter and bolometer simultaneously. Making use of this feature, the RS can be independently calibrated, replacing the microwave electric field in the sensor by a dc electric field the strength of which can be measured with high accuracy.

The readings of two sensors calibrated in such a way were compared with the readings of the Russian (former Soviet Union) pulse power standard. The measurements were performed for 18 years, starting in 1982. During this long-term experiment, some change in the sensitivity within ±4% was observed. Bearing in mind that the main error of the standard was ±4%, it becomes clear that the tested sensors demonstrate very good long-term stability.

3.2. Diaphragm-type RS

Improving thermal characteristics of the sensor and widening its possible applications for HPM pulse measurements, the diaphragm-type RS shown in Fig. 1b was developed. It is seen that in this case the SE is placed in the center of the waveguide between a thin metal foil and the wide wall of the waveguide. The length of the SE roughly corresponds to 1/10th of the waveguide's narrow wall.

The diaphragm-type RS has at least two advantages over the cross-waveguide-type RS. First, by decreasing the length, the thermal characteristics of the SE are improved. Second,

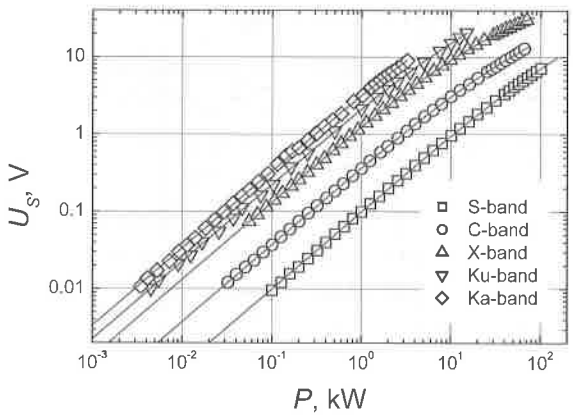

Fig. 2. Output signal dependences on microwave power for the RS designed for short HPM pulse measurement at different frequency bands. Points denote experimentally measured values using a dc pulse supply producing a 50-V dc drop on the SE, and solid lines correspond to the polynomial approximation [Eq. (7)].

because the SE occupies only a part of the waveguide window, a smaller reflection from it can be expected even though a lower-specific-resistance semiconductor is used for the manufacturing of the SE.

Diaphragm-type RSs have been manufactured and tested beginning from L up to Ka band. They are used in Russian, Swedish, U.S., and other laboratories dealing with HPM pulses. The RS found application for the measurement of HPM pulse power density in free space. A RS connected to a horn antenna from one side and to a matched load from the other comprises a unit that is able to measure pulse power density up to a few megawatts per square meter.[1] The measurements were carried out in an anechoic chamber driven by the Microwave Test Facility at SAAB Military Aircraft, Sweden.

The diaphragm-type RS has been upgraded for the measurement of nanosecond-duration HPM pulses. RSs from S to Ka band have been manufactured, calibrated, and tested. The output signal dependencies on pulse power are shown in Fig. 2. It is seen that using dc pulse feeding, output signals up to 30 V are obtained. It should be pointed out that the RS has been calibrated up to pulse power levels available in the laboratory. RS can likely be used at higher pulse power levels, ultimately limited by air breakdown in the waveguide.

We estimated a response time of the RS using the time domain reflectometry method. The sensor is fed by a dc pulse with a subnanosecond rise time, and by measuring the duration of the transient formed by the initial and reflected pulse, the response time of the RS was estimated. Measurement results for the different-band RS are collected in Table 2. As one can see from the third column of the table, where the ratio of the response time to the average period of the oscillations in the waveguide's frequency band is presented, the manufactured RS can measure microwave pulses with durations on the order of a few tens of periods of microwave oscillations. It was confirmed by tests of the X-band RS using short HPM pulses generated by a backward wave oscillator driven by the SINUS-6 electron beam accelerator at the University of New Mexico.[2]

The main drawback of the waveguide-type RS for short HPM pulse measurement is a large variation of the sensitivity [Eq. (5)] in a waveguide's frequency band. It was determined

Table 2. Measured time responses for the different-band RS

Band	τ, ns	τ/T
S	2.5	8
C	2	10
X	0.5	5
Ka	0.4	7
Ku	0.2	7

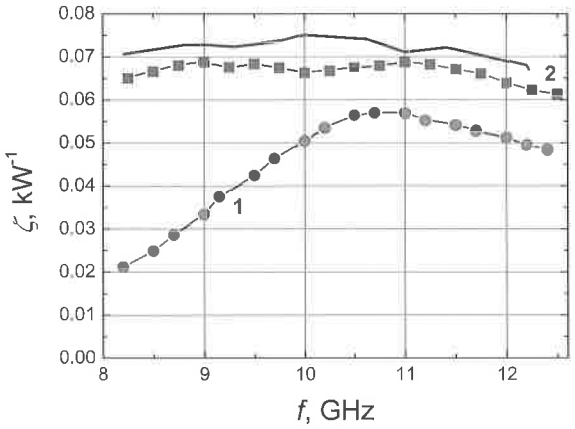

Fig. 3. Dependencies of the sensitivity on frequency for the initial (1) and optimized (2) X-band diaphragm-type RS. Points show measurement results, and the solid line shows the theoretical prediction.

that the sensitivity of the X-band RS changes in the frequency band by more than a factor of two (Fig. 3). The same frequency response is likely to be characteristic of the RS in other frequency bands as well. Bearing in mind this drawback of the waveguide-type RS, we performed investigations of factors influencing frequency response.

Making use of the FDTD method,[8] the peculiarities of the interaction of the semiconductor sample inserted under a thin metal diaphragm in the waveguide were investigated. It was shown that the average electric field strength in the SE is influenced by a resonance phenomenon.[6] The resonance occurs when the effective length of the diaphragm for the wave propagating under it becomes a whole number of half-waves. Varying the electrophysical parameters of the diaphragm-type RS (diaphragm length, dimensions, and specific resistance of the SE) and taking into account that the resistance of the RS should be less than or equal to 50 Ω, the optimal set of parameters providing the smallest possible sensitivity variation in the waveguide's frequency band was determined. A maximum-to-minimum-sensitivity ratio of 1.09 was found for the optimal set of parameters.

Theoretical predictions were proven experimentally. Experimentally measured frequency responses of the initial and optimized RS are shown in Fig. 3. It is seen that the optimized

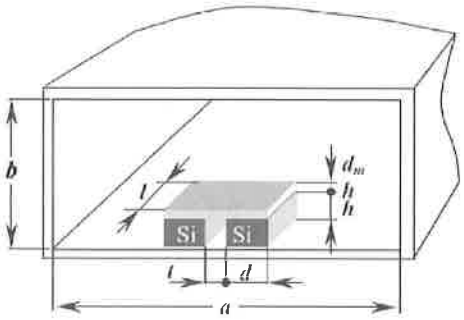

Fig. 4. Schematic view of the RS for millimeter-wave band.

RS is characterized by a smooth dependence of the sensitivity on frequency. Experimentally measured sensitivity variation is roughly ±6% in the waveguide's frequency range. That is sufficiently close to the theoretically predicted value of 1.09. The absolute value of the measured sensitivity coincides well with the calculated one. A small difference between them can be attributed to size tolerances between the actual device and modeled prototype, to small mechanical displacements when installing the SE under the diaphragm, and to measurement errors.

3.3. RS for millimeter wave

High-power microwave pulse generation techniques progressed rapidly toward higher frequencies in recent years.[9] This imposes new requirements for sensors that can be used for the measurement of HPM pulses in the millimeter-wave region. One of the possible solutions is the RS. Unfortunately, the most successful concept of the diaphragm-type RS could not be directly downscaled to the millimeter-wave region due to the small dimensions of the waveguide. For the measurement of high-power millimeter-wave pulses in the frequency range 78–118 GHz (W band, waveguide window 2.54 × 1.27 mm^2), we propose a new concept of the SE consisting of two separate samples mounted in the center of the wide wall of the waveguide in close proximity to each other, as shown in Fig. 4. Their upper contacts are shorted with a metal foil. The lower contact of one of the sensors is grounded, whereas the other one is isolated. It is used for RS feeding and output signal measurement. To measure pulse power, the RS is connected into a dc circuit with a current source. Thus, SEs are connected in series with respect to the dc circuit but in parallel with respect to the millimeter-wave electric field.

We performed FDTD simulations in order to investigate the interaction of such a semiconductor structure with millimeter waves. It was found that some resonances occur in the SE when increasing its length in a wave propagation direction. Making use of the interplay between half-wavelength resonance in the structure and the conductivity current in it, the increase in the average electric field in the sensor with frequency was compensated by the electric field decrease in the waveguide because of waveguide dispersion and the decrease in the electron-heating effect with frequency [Eq. (3)]. Thus, the RS having nearly independent sensitivity with frequency in a waveguide's frequency band has been proposed. The details of the simulations were published by Kancleris et al.[5]

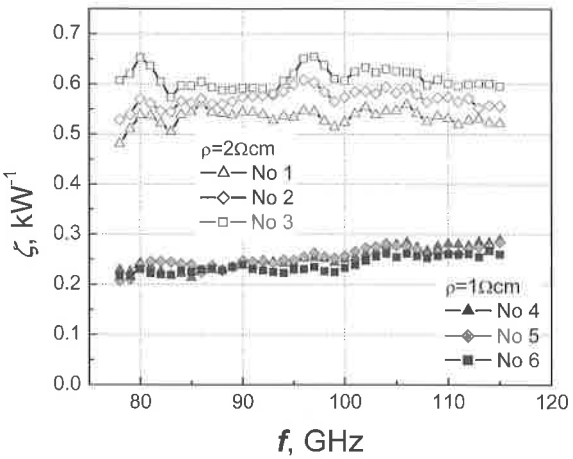

Fig. 5. Experimentally measured dependencies of the sensitivity on frequency for both groups of the RS for millimeter-wave band.

The RS with optimal dimensions of the SE (height $h = 0.1$ mm, width $d = 0.15$ mm, length in the wave propagation direction $l = 0.6$ mm) was manufactured. The surface-mounted device technology of component soldering was applied to fix SEs on polished metal disks, which in turn were mounted into waveguide holders. Thus, finally the RS was manufactured as a section of a W-band waveguide with the SEs inside. Two groups of SEs with optimal dimensions were made from different specific-resistance n-Si wafers, namely, $\rho = 1\ \Omega$ and $-2\ \Omega$ cm with nominal dc resistances of 11 and 22 Ω, respectively. For final tests, three sensors from each group were chosen.

The sensitivity, voltage standing wave ratio (VSWR), and insertion loss dependencies on frequency were measured using a low-power tunable millimeter-wave source, reference wattmeter, and lock-in amplifier. It was found that VSWR is less than 1.25 and insertion loss -0.8 dB for the RS of both groups in the frequency range 78–118 GHz. Results of the measurements of the dependence of sensitivity on frequency are presented in Fig. 5.

It is seen that the sensors of the second group are more sensitive than those of the first one. Such behavior was predicted by our theoretical considerations.[5] Taking into account the finite thickness of the metal foil d_m shorting upper contacts and an air gap t between SEs, a reasonable agreement between measured and calculated values of sensitivity was obtained (refer to Fig. 4). Details of the comparison were published by Kancleris et al.[4] From experimental results it is seen that the measured sensitivity variation within the waveguide frequency range was $\pm 15\%$ for the first group and $\pm 8\%$ for the second one. This is a very good result because the Agilent sensor W8486A available on the market and devoted to average power measurement demonstrates a $\pm 15\%$ sensitivity variation in a 3-mm-wave band.

The dependencies of the output signal on the pulse power were measured up to 2 kW using a magnetron operating at 94 GHz. The duration of millimeter-wave pulses was 300 ns. To get a high output signal, the RS was fed by a pulsed-current source producing a 10-V drop on the SEs. At a maximum pulse power, the output signal was roughly 1.5 V for the RS of the first group and exceeded 2 V for the second one. From the experimental data, the dependence of the relative resistance change of the RS on the pulse power was

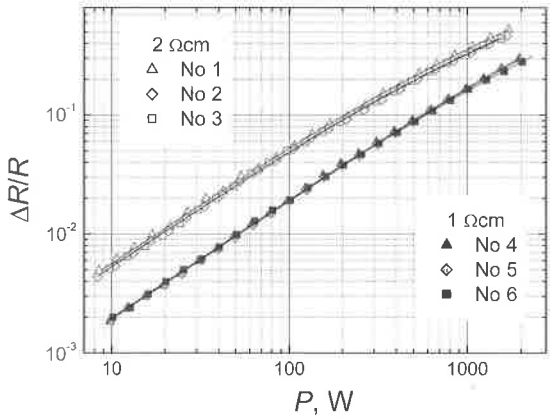

Fig. 6. Dependencies of the relative resistance change on pulse power for both groups of the RS at $f = 94$ GHz. Points show measurement results, and solid lines demonstrate two-term approximations [Eq. (7)].

determined. These results are shown in Fig. 6. It is seen that at a maximum pulse power, the largest value of $\Delta R/R$ was about 30% for the first group of the RS and 50% for the second one. Bearing in mind that at a lower frequency the RS was successfully employed up to a twofold increase in the resistance, one can expect that the present RS could register even higher pulses of millimeter waves.

4. Coaxial-Type RS

The application of the waveguide-type RS is restricted by the bandwidth of certain waveguides. Hence, for the HPM pulse measurement in a wide frequency range a set of sensors has to be used. Therefore, the measurement system becomes complicated and its cost increases. Moreover, at a lower frequency the size and weight of the waveguide section with the RS increase and it becomes inconvenient to use. These reasons pushed us to develop a coaxial-type RS (CRS) that can be used in a wider frequency range.

A schematic block diagram of the CRS is shown in Fig. 7. It is seen that the CRS was designed as a two-terminal device. One of them will be used to connect the sensor to a coaxial line where the measuring microwave pulse is propagating. The other one connects the CRS to the measuring circuit and sensor-feeding unit. The CRS was designed on the

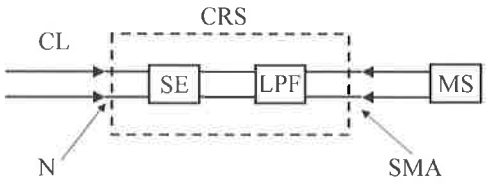

Fig. 7. Schematic block diagram of the CRS: SE, sensing element; LPF, low-pass filter; CL, coaxial line; N, N-type connector; SMA, SMA-type connector; and MS, sensor's feeding and measuring system.

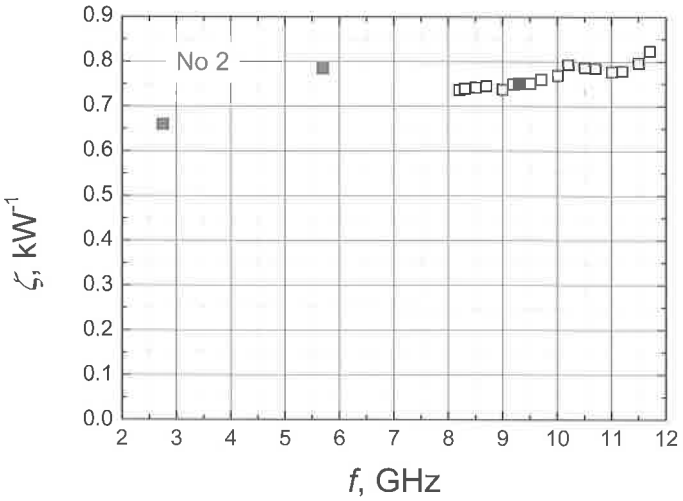

Fig. 8. Dependence of the sensitivity of the CRS on frequency. Solid points demonstrate measurement results using magnetron generators, and open points show measurement results using X-band TWT.

basis of a 50 Ω impedance coaxial line. It actually consists of the SE and a low-pass filter. One contact of the SE is directly connected to the center core of the coaxial line, whereas the other one is connected to the shield. Therefore, the SE serves as a matched load and a pulse power detector simultaneously. To achieve good matching of the CRS with the coaxial line, the resistance of the SE is set to be 50 Ω. Because the dimensions of the SE are chosen to be much smaller than the wavelength of the microwave, the SE might be considered as a lumped element of the circuit. This is why a good matching might be achieved in a wide frequency range. The main purpose of the low-pass filter of the CRS is to prevent the direct propagation of the microwave pulse to the measuring unit. At the same time, the low-pass filter should not spoil the matching of the SE with the coaxial line in a wide frequency band. Finally, the parameters of the low-pass filter influence the response time of the CRS. Therefore, all three factors should be taken into account when choosing the parameters of the low-pass filter.

As the low-pass filter, we employed a five-element Butterworth filter. Filters made from lumped elements and from the sections of a microstrip line and a hybrid filter were tested. In the hybrid filter the first element of the filter, the inductance, was partly replaced by a conductor coated by a layer of ferrite. This improves significantly the performance of the filter in the high-frequency region, providing measurements of the microwave pulses in the frequency range 2–12 GHz. The measured frequency response of the CRS with the hybrid filter is shown in Fig. 8. Solid points in the figure show results obtained at fixed frequencies using magnetron generators, and open points demonstrate results measured using X-band TWT. It is seen that the sensitivity of the CRS is slightly growing with frequency, and from 2.7 to 11.7 GHz, it increases by a factor of 1.25. The measured VSWR was less than 1.6 within the considered frequency range.

The output signal dependence of the CRS on the pulse power measured up to 1 kW at 9.3 GHz is shown in Fig. 9. A dc source producing a 4-V drop on the SE was used. It is seen that the output signal at maximum pulse power exceeds 1.5 V.

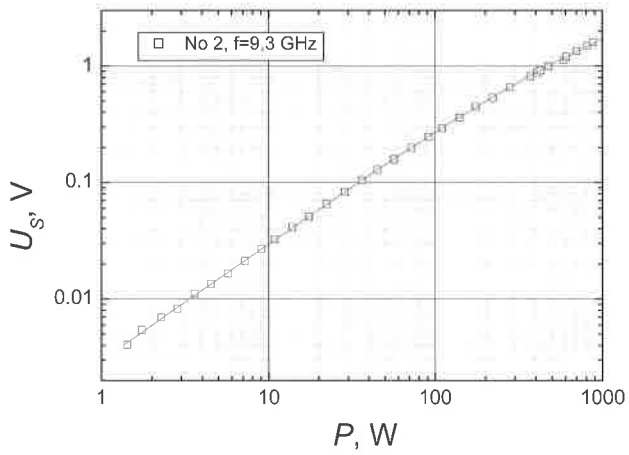

Fig. 9. Dependence of the output signal on pulse power at $f = 9.3$ GHz and $U_0 = 4$ V for the CRS with hybrid filter. Points show experimentally measured results, and the solid line corresponds to the polynomial approximation [Eq. (7)].

5. Conclusions

The RS, based on the electron-heating effect in semiconductors, is one of the most promising devices for HPM applications. The RS can measure 40–60-dB-higher pulse power in comparison with a conventional diode. It can be used in a wide frequency range for which powerful HPM pulse sources are now designed and manufactured. The RS demonstrates very good long-term stability and is resistant to large power overloads. Using the dc pulse supply for the RS feeding, an output signal up to a few tens of volts can be obtained without any amplification circuit. The RS can be made sufficiently fast to measure microwave pulses with a duration of the order of a few tens of periods of microwave oscillations. Making use of the increase in the electric field in the SE with frequency due to a resonance phenomenon, a sufficiently flat frequency response of the RS in the waveguide's frequency band can be engineered, compensating not only the decrease in the electric field due to waveguide dispersion but also the decrease in the electron-heating effect with frequency.

6. Acknowledgments

The Lithuanian State Science and Studies Foundation supported this work through the programs "Sensors" and "Advanced Millimeter-Wave Electronics." The effort was sponsored by the Air Force Office of Scientific Research, Air Force Material Command, USAF, under grants F61775-02-WE030 and FA8655-04-1-3047. The authors would like to thank Dr. T. Anbinderis, General Director of Joint Stock Company "Elmika," Vilnius, Lithuania, for fruitful cooperation in testing of the millimeter-wave RSs.

References

[1]Dagys, M., Ž. Kancleris, V. Orševskij, R. Simniškis, M. Bäckström, U. Thibblin, and B. Wahlgren, IEEE Trans. Microw. Theory Tech. **43**, 1379 (1995).

[2]Dagys, M., Ž. Kancleris, R. Simniškis, E. Schamiloglu, and F.J. Agee, "Application of Resistive Sensors for Short High-Power Microwave Pulse Measurement," 12th IEEE Int. Pulsed Power Conf. Proceedings on CD, Monterey, CA, pp. 829–832, June 27–30, 1999.

[3]Dagys, M., Ž. Kancleris, R. Simniškis, E. Schamiloglu, and F.J. Agee, IEEE Antennas Propag. Mag. **43**(5), 64 (2001).

[4]Kancleris, Ž., R. Simniškis, M. Dagys, and V. Tamošiūnas, IET Microw. Antennas Propag. **1**(3), 757 (2007).

[5]Kancleris, Ž., V. Tamošiūnas, M. Dagys, R. Simniškis, and F.J. Agee, IEE Proc. Microw. Antennas Propag. **152**(4), 240 (2005).

[6]Kancleris, Ž., V. Tamošiūnas, M. Dagys, R. Simniškis, and F.J. Agee, IEEE Microw. Wireless Components Lett. **16**(7), 422 (2006).

[7]Ryder, E. J., and W. Shockley, Phys. Rev. **81**, 139 (1951).

[8]Taflove, A., *Computational Electrodynamics: The Finite-Difference Time-Domain Method.* Artech House, Norwood, MA (1995).

[9]Thumm, M., Int. J. Infrared Millim. Waves **26**(4), 483 (2005).

[10]Yang, K., G. David, S.V. Robertson, J.F. Whitaker, and L.P.B Katehi, IEEE Trans. Microw. Theory Tech. **46**(12), 2338 (1998).

The Authors

Dr. Mindaugas Dagys graduated from Vilnius Technical University in 1970 and received an M.S. degree in electronics. He received a Ph.D. degree in microwave pulsed power measurement in 1980. He has published about 80 scientific papers and is a coauthor of 9 inventions. At the present time he is senior research associate of the Semiconductor Physics Institute. He has been a member of the IEEE since 1995. His research interests lie in microwave measurements metrology and diagnostics. He designed microwave sensors and instruments based on hot-electron phenomena in semiconductors. Developed instruments have been used in scientific centers in Sweden, Russia, Germany, and the United States.

Dr. Žilvinas Kancleris graduated from Vilnius University and received an M.S. degree in physics in 1969. He received Ph.D. and Doctor of Science (Doctor Habilitatus) degrees in physics from Vilnius University in 1976 and 1990, respectively. Upon graduation he joined the Semiconductor Physics Institute as a Research Fellow and now is a head of the Microwave Laboratory. He has more than 100 scientific publications and has coauthored 3 monographs (in Russian) about hot electrons. His research interests are in the investigation of nonlinear transport in semiconductors and the application of this effect for microwave pulse power measurement, computational methods, and modeling. He is a member of the IEEE, the Lithuanian Physical Society, and the European Physical Society.

Dr. Rimantas Simniškis graduated from Kaunas Technical University in 1978 and received an M.S. degree in technology and design of radio equipment. He received a Ph.D. degree in microwave measurements in 1992. At the moment he is a senior research associate at the Microwave Laboratory, Semiconductor Physics Institute. His research is focused on the development of sensors, instruments, and testing systems for high-power microwave applications. He has published more than 50 publications on high-power pulse measurements and presented results at international conferences. Sensors and testing systems that he developed are used in high-power test facilities in Sweden, the United States, Russia, Germany, India, and Taiwan.